Direct evidence for anisotropic three-dimensional magnetic excitations in a hole-doped antiferromagnet

Rajesh Dutta,[1,2,*] Avishek Maity,[3,4,†] Anna Marsicano,[5] J. Ross Stewart,[6] Matthias Opel,[7] and Werner Paulus[5]

[1]*Institut für Kristallographie, RWTH Aachen Universität, 52066 Aachen, Germany*
[2]*Jülich Centre for Neutron Science at Heinz Maier-Leibnitz Zentrum, 85747 Garching, Germany*
[3]*Institut für Physikalische Chemie, Georg-August-Universität Göttingen, 37077 Göttingen, Germany*
[4]*Heinz Maier-Leibnitz Zentrum, Technische Universität München, 85747 Garching, Germany*
[5]*Institut Charles Gerhardt Montpellier, Université de Montpellier, 34095 Montpellier, France*
[6]*ISIS Neutron and Muon Source, Rutherford Appleton Laboratory, Didcot OX11 0QX, United Kingdom*
[7]*Walther-Meißner-Institut, Bayerische Akademie der Wissenschaften, 85748 Garching, Germany*

(Received 6 July 2020; accepted 28 September 2020; published 15 October 2020)

We report a neutron-scattering study on $Pr_{2-x}Sr_xNiO_4$ ($x \approx 0.5$) with magnetic incommensurability $\epsilon = 0.461$ at 10 K, showing direct evidence for out-of-plane magnetic excitations caused by a non-negligible interlayer spin coupling ($J_\perp$). The magnetic spectrum is fully represented by linear spin wave theory considering an unconventional body-centered-like stacking of discommensurated spin stripes. A large easy-plane-type single-ion anisotropy (≈1.5 meV) has been found to be responsible for a finite-energy (≈13 meV) Goldstone mode at the magnetic zone center. Our results validate the presence of a sizable out-of-plane interaction resulting in an anisotropic three-dimensional nature of spin dynamics in $Pr_{2-x}Sr_xNiO_4$ near the half-doped region.

DOI: 10.1103/PhysRevB.102.165130

I. INTRODUCTION

Long-range three-dimensional (3D) antiferromagnetic (AFM) ordering has been observed in both stoichiometric 214-type nickelates and cuprates. Hole doping in the normal state of high-T_c La-based cuprates partially suppresses 3D AFM ordering [1,2], whereas studies on La-based nickelates suggest hole doping leads to a strong two-dimensional (2D) charge and spin ordering [3,4]. Most of the previous studies [5–8] have predominantly suggested hole-doped 214-type nickelates to be quasi- or purely two-dimensional antiferromagnets neglecting the possible out-of-plane interactions in between the interlayer stripes, and accordingly the related effects on the in-plane excitations have not been discussed. In the previous study on half-doped $Pr_{2-x}Sr_xNiO_4$ [9] a sizable out-of-plane interaction ($J_\perp$) was predicted by linear spin wave theory (LSWT). However, it is very important to understand whether the presence of such out-of-plane interaction is common for any underlying spin microstructure in $Pr_{2-x}Sr_xNiO_4$.

Here we present an inelastic neutron scattering (INS) study on $Pr_{1.5}Sr_{0.5}NiO_4$ single crystals, but with another $\epsilon = 0.461$, i.e., a significantly different underlying spin microstructure compared to the previous study ($\epsilon = 0.4$). Our results provide a detailed picture of the $[Q_{x,y},Q_z]$ dependence of the spin excitations in $Pr_{1.5}Sr_{0.5}NiO_4$ over several Brillouin zones presenting its anisotropic three-dimensional nature which has never been realized experimentally before in 214-type nickelates. The magnetic spectrum is adequately described in an unconventional model of two-layer stacking of discommensurated spin stripe (DCSS) NiO_2 planes along the c axis. Our results signify that the presence of L-dependent spin dispersion is more likely to be common at least in Pr-based 214 nickelates near half-doping while the in-plane exchange interactions and the presence of single-ion anisotropy are highly dependent on the underlying spin microstructure.

II. METHODS AND GENERAL CONSIDERATIONS

A single crystal of $Pr_{1.5}Sr_{0.5}NiO_4$ was grown using the traveling solvent floating zone method [10]. INS experiments were carried out at the thermal triple-axis spectrometer PUMA [11] and time-of-fight spectrometer MAPS [12]. A complete description of experimental configurations and data analysis is given in the Supplemental Material [13]. The observed spin stripe incommensurability $\epsilon = 0.461$ in our half-doped $Pr_{1.5}Sr_{0.5}NiO_4$ can be represented by a DCSS NiO_2 layer consisting of an alternating arrangement of one 1/3-stripe and five checkerboard (CB) units as in Fig. 1(a), where we have considered the average unit cell parameters in the pseudotetragonal lattice $F4/mmm$ with $a = b = 5.4$ Å and $c = 12.54$ Å. The spin stripe ordering takes place below $T_{SO} \approx 130$ K (see Fig. S1 in the Supplemental Material [13]). In nickelates, the stripes run diagonal to the Ni-O-Ni bonds and magnetic wave vectors are defined as $\mathbf{q}_{so} = (1 \pm \epsilon, 0, 0)$ [15–17] where the coordinates are in reciprocal lattice units $(2\pi/a, 2\pi/b, 2\pi/c)$.

*Corresponding author: rajesh.dutta@frm2.tum.de
†Corresponding author: avishek.maity@frm2.tum.de

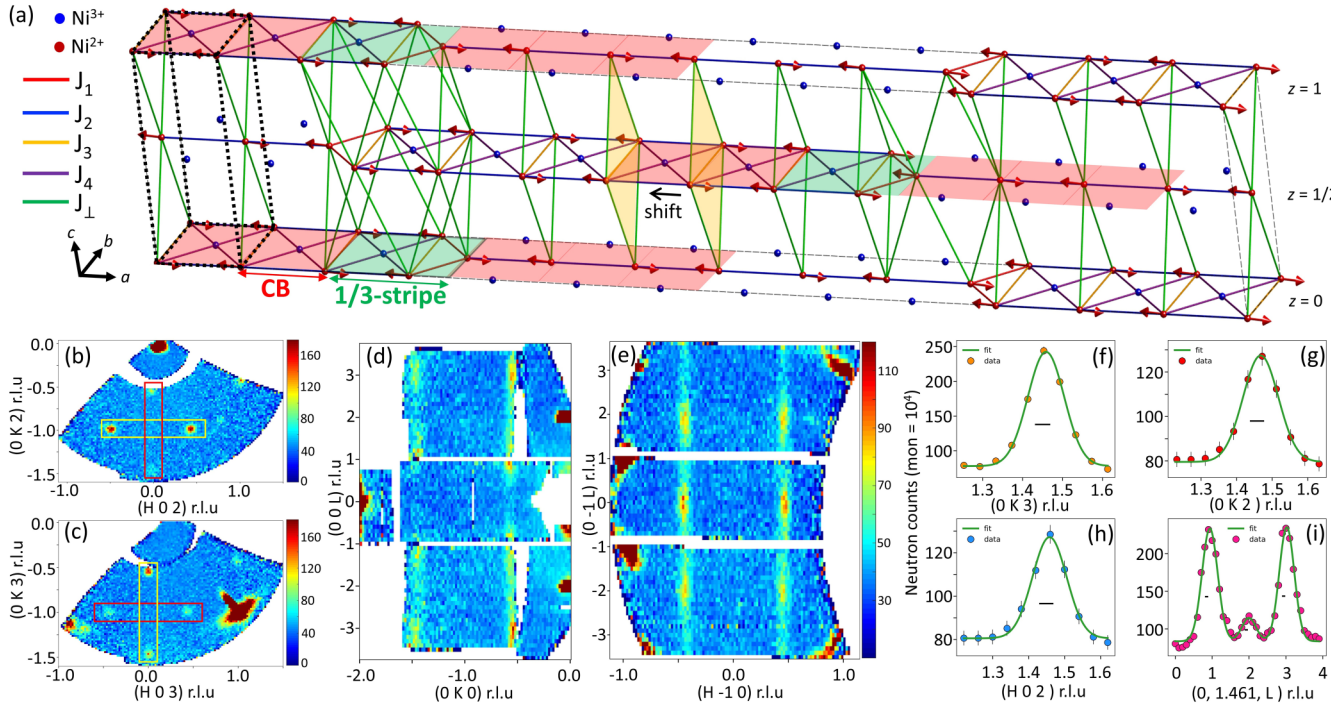

FIG. 1. Spin stripe discommensuration in $Pr_{1.5}Sr_{0.5}NiO_4$. (a) DCSS unit cell corresponding to the magnetic incommensurability $\epsilon = 0.461$ for one twin domain. The average chemical unit cell ($F4/mmm$) is indicated in black dashes. Green and red shading represents 1/3-stripe and CB unit, respectively. For the other orthogonal twin domain the model is exactly the same but rotated by 90° around the c axis. Magnetic exchange interactions are indicated by the solid lines in different colors. (b), (c) 2D cuts of ($HK2$) and ($HK3$) planes, obtained using the HORACE software [14] from wide crystal-rotation-scan (80° around the vertical c axis) data at MAPS with incident neutron energy $E_i = 60$ meV, representing four elastic spin order peaks modulated from (0, −1, L = integer) AFM zone centers. Yellow and red boxes indicate respectively the strong and weak intensity variation along L. (d), (e) 2D slices of ($0KL$) and (H-1L) planes showing the intensity variation of the spin order peaks along L. (f)–(i) Elastic scans through the AFM zone centers in different L planes from data measured at PUMA confirming the magnetic incommensurability $\epsilon = 0.461$ and the intensity variation in different L. Horizontal bars represent the instrumental resolution and vertical lines are error bars.

III. RESULTS AND DISCUSSION

2D cuts of ($HK2$) and ($HK3$) planes at $E = 0$ meV in Figs. 1(b) and 1(c) show the intensity of the spin satellites modulated along H are strong in L = even planes and weak in L = odd planes, and vice versa for the satellites along K. This becomes even more comprehensible from the ($0KL$) and (H-1L) planes in Figs. 1(d) and 1(e). These planes contain well-separated strong intensities centered on L = integer positions showing a 3D correlation of the magnetic ordering. Gaussian fitted FWHMs of the scans along H, K is about 0.095 ± 0.003 r.l.u. in Figs. 1(f)–1(h) and along L is about 0.5 r.l.u. in Fig. 1(i). The instrumental Q resolution is calculated to be $\approx 0.045 \pm 0.002$ Å^{-1} at the elastic limit using the Eckold-Sobolev algorithm [18] for the used configuration of PUMA. From these values the estimated in- and out-of-plane correlation lengths are $\xi_{H,K} \sim 19$ Å and $\xi_L \sim 8.4$ Å, respectively, which indicate a short-range nature of the 3D ordering. The intensity ratio of the strong and weak spin peaks within and in between the L planes is about 3:1. Please note that as the intensity ratio between the weak and strong spin satellites alternates for different L, this cannot be related to only the twin volume fraction. Instead we found that stacking of NiO_2 planes along L plays the most important role. Since no extinction of the magnetic reflections was observed for L = integer, the DCSS layer at $z = 1/2$ has been shifted towards the left [indicated by the black arrow in Fig. 1(a)] by one chemical unit cell from the ideal body-centered-like stacking to match the observed intensities of the magnetic reflections taking into account the equal volume fraction. Such intensity variation is directly linked to the specific 3D stacking of the NiO_2 layers (see Fig. S2 in the Supplemental Material [13] for a comparison to ideal body-centered-like stacking).

Figure 2 summarizes the measured and calculated in-plane magnetic excitations up to 50 meV energy transfer. To explain the observed spin excitation spectra, we have performed a LSWT-based calculation via the SPINW code [19] using a generalized Heisenberg spin only Hamiltonian given as

$$H = \sum_{i,j} J_{ij}\left(S_i^x S_j^x + S_i^y S_j^y + S_i^z S_j^z\right) + \Lambda \sum_i \left(S_i^z\right)^2, \quad (1)$$

where the indices i and j run over all the lattice sites of Ni^{2+}, J_{ij} represents all possible isotropic Heisenberg exchange interactions acting on Ni^{2+} spins, and $\Lambda > 0$ is the easy-plane single-ion anisotropy (EPSIA) constant. We have incorporated the DCSS unit cell shown in Fig. 1(a) for our spin wave calculation with a fair assumption of local spin arrangements to be collinear in the NiO_2 planes like other homologous compounds [9,20,21]. Although SPINW assumes long-range

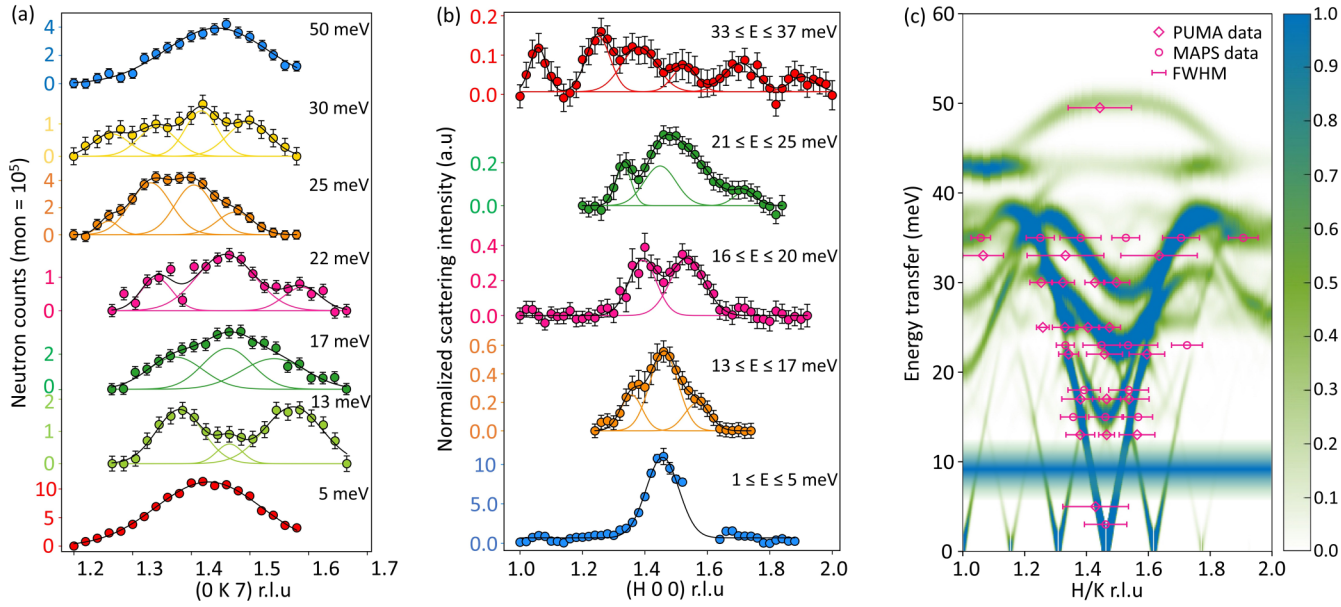

FIG. 2. In-plane magnetic excitations in discommensurated $Pr_{1.5}Sr_{0.5}NiO_4$ at 10 K. (a) Constant-E scans performed at PUMA using final neutron energy of $E_f = 14.68$ meV. All the scans are measured along K through the (0, 1.461, 7) magnetic zone center. (b) Constant-E scan profiles integrated within an energy range of $\Delta E = \pm 2$ meV for a K range of $\Delta K = \pm 0.1$ reciprocal lattice units (r.l.u.) and obtained from narrow crystal-rotation-scan ($\pm 3^\circ$ around the vertical a axis, keeping the c axis almost parallel to the neutron beam) data measured at MAPS with incident neutron energy $E_i = 60$ meV. All the scans are background subtracted and fitted with multiple Gaussian profiles. (c) Intensity convoluted in-plane spin wave spectra with overplotted magnetic wave vectors and full widths at half maximum (FWHMs) as horizontal bars. The strong crystal-electric-field excitation observed in the measurement is indicated in blue green shading in the energy range 6–13 meV. No constant-E scans were performed on PUMA in this energy range. In (a) and (b) vertical lines represent error bars.

spin order for LSWT calculation, still we have obtained a satisfactory agreement with the experimental observation in our case where the spin correlations are relatively short. But it is worth mentioning that the effect of short-range spin correlation might broaden the spin dispersion without giving rise to any extra modes [22]. From a least-squares fit of the spin dispersion we have obtained the refined in-plane exchange interactions of $J_1 \approx 14.0$, $J_2 \approx 0.1$, $J_3 \approx -0.05$, and $J_4 \approx 6.7$ meV, and out-of-plane interaction $J_\perp \approx 2.2$ meV and $\Lambda \approx 1.5$ meV. In the low energy range (<5 meV) the acoustic branches dispersing from the magnetic satellites cannot be resolved separately. Instead they appear as broad peaks due to the limitation of instrumental resolution. We cannot confirm whether this broadening is due to the disorder (short-range magnetic correlation) as the instrumental Q resolution in this energy range is already larger than the calculated splitting between the two branches of the acoustic mode (gapless Goldstone mode). In addition another finite-energy Goldstone mode arises at the same AFM zone center with an energy gap of 13 meV due to the EPSIA. It is worth noticing that no EPSIA was observed in the previous study ($\epsilon = 0.4$) [9]. The optical modes in the energy range 22–38 meV result solely from the out-of-plane interaction. In the absence of $J_\perp$, all the corresponding modes will collapse with a maximum energy of the dispersion up to 40 meV which is contradictory to the experimental observation, i.e., 50 meV (Fig. S3a in the Supplemental Material [13]). Simply increasing the in-plane interactions without considering $J_\perp$ does not match the measured spin dispersion. The overplot of the measured magnetic wave vectors on the calculated dispersion in Fig. 2(c) shows an impressive agreement between the measurements and the calculated dispersion. In addition, we have also estimated the out-of-plane exchange interaction by following the analytical expression below [23–25]:

$$(M_s/M_t)^2[\xi(T_{so})/a]^2 J_\perp \approx K_B T_{so}, \tag{2}$$

where M_s is Ni^{2+} sublattice magnetization ($\approx 1.5\mu_B$) and $M_t = g\mu_B$, ξ is the in-plane spin correlation length at the spin ordering temperature T_{so}, a is the lattice constant of the chemical unit cell, and K_B is the Boltzmann constant. Plugging the corresponding values in Eq. (2), we obtain $J_\perp \approx 1.9$ meV, which is quite similar to the value obtained from the spin dispersion fit. It is worth mentioning that following Eq. (2) the estimated $J_\perp$ interaction in La_2CuO_4 ($\sim$0.007 meV) is much smaller than that in $Pr_{1.5}Sr_{0.5}NiO_4$ ($\sim$2.2 meV), indicating that the typical in-plane correlation length in nickelates is much smaller than in cuprates (Fig. S4 in the Supplemental Material [13]).

A remarkable result of our study is the direct observation of the out-of-plane excitations presented as a composite image in Fig. 3. A series of constant-E scan profiles along L are displayed in Figs. 3(a)–3(d). The spin wave dispersion calculated along L is in a good agreement with the experiments as can be seen from the overplotted peak positions in Fig. 3(e). Even the weak acoustic modes dispersing from the corresponding weak spin peaks are clearly visible in the scan profile at $\sim$6 meV. The acoustic branches of the out-of-plane excitations disperse with a maximum energy of 25 meV. The rest of the optical-like modes are the same as described in the in-plane excitations in Fig. 2(c). For clarity see the combined in- and out-of-plane spaghetti plot in Fig. S3 in the Supplemental Material [13]. Even though the statistics of the data collected during the

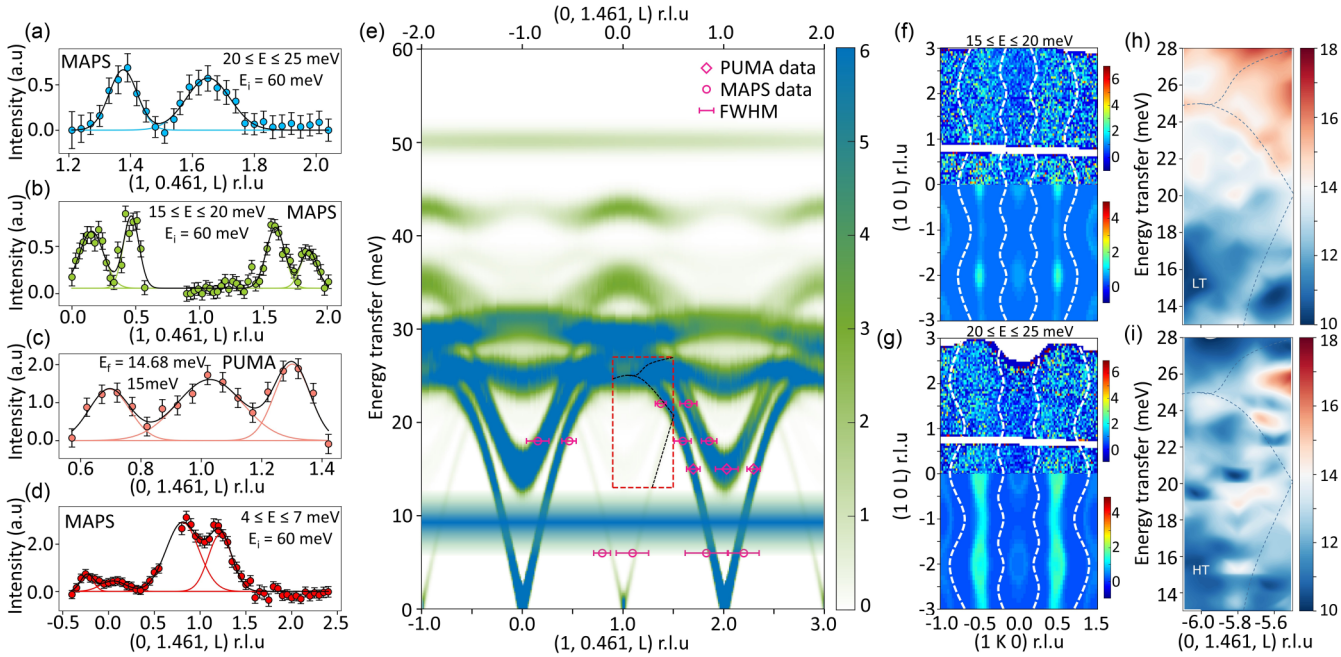

FIG. 3. Out-of-plane magnetic excitations in discommensurated $Pr_{1.5}Sr_{0.5}NiO_4$ at 10 K. Data in this figure are measured at MAPS (wide crystal rotation scan) using incident neutron energies $E_i = 60$ meV, and at PUMA using a final neutron energy of $E_f = 14.68$ meV. (a)–(d) Constant-E scan profiles along L at two orthogonal spin satellite positions $(0, 1.461, L)$ and $(1, 0.461, L)$. All the scans are background subtracted and fitted with multiple Gaussian profiles to extract the magnetic wave vectors. Vertical lines represent the error bars. (e) Calculated out-of-plane excitations with overplotted magnetic wave vectors and FWHMs as horizontal bars. Please note that the spin wave modes are the same for both satellites as indicated by the two different x axes. The bottom axis corresponds to those data measured along $(1, 0.461, L)$ where modes from $L =$ even peaks are strong. The top axis represents the data along $(0, 1.461, L)$, where modes from $L =$ odd peaks are strong. (f), (g) Two constant-E slices of $(1KL)$ plane from MAPS (top) presented with their corresponding simulations (bottom). White sinusoidal-like dashed lines are visual guides for the inelastic intensity distribution. (h), (i) Low- and high-T maps of the out-of-plane excitations measured at PUMA for the rectangular section of the L dispersion indicated by red dashes in (e). Lines in black dashes are visual guides for the magnon modes of L dispersion.

wide crystal rotation scan at MAPS was not enough, two constant-E slices of the $(1KL)$ plane in Figs. 3(f) and 3(g) clearly show the dynamical features which resemble the corresponding simulations. More importantly, in order to confirm the magnetic origin of the out-of-plane excitations, we have carried out temperature-dependent mapping of a small section of the L dispersion [indicated in Fig. 3(e)] at 10 and 300 K which are presented in Figs. 3(h) and 3(i), respectively, where the intensity represents the scattering cross section $S(Q, E)$ without any Bose factor correction. Both acoustic and optical modes are clearly visible at 10 K and disappear at 300 K.

The in-plane (ip) and out-of-plane (oop) magnon bandwidth of the acoustic modes ($\Delta E_{ip} \approx 38$ meV and $\Delta E_{oop} \approx 25$ meV) and their corresponding spin wave velocities are direct measures of the anisotropic nature of the magnetic excitations. We have evaluated spin wave velocities $v_{ip} \approx 177 \pm 12$ meV Å and $v_{oop} \approx 90 \pm 7$ meV Å via a linear least-squares fit of magnetic wave vectors corresponding to the acoustic modes in the low-energy regime. These values are consistent with our analytical calculations following the simple approximation [26,27] from Chakravarty, Halperin, and Nelson (CHN) renormalization group theory [28,29] for the quantum Heisenberg antiferromagnets. Spin wave velocity then can be written as $v = Z_c(S)2\sqrt{2}JSa$ where in our case we have considered effective in-plane exchange coupling $J \equiv J_{\text{eff}} \approx 10.35$ meV since we have a mixture of stripe and CB units rather than a pure Néel AFM ordering. Here, $Z_c(1) = 1.0843$ is the renormalization factor for the spin wave velocity in $S = 1$ systems and a is the lattice constant. Using these values we obtained $v_{ip} \approx 171$ meV Å. We have applied the same equation for the out-of-plane spin wave velocity where $J \equiv J_\perp \approx 2.2$ meV, lattice constant $c \approx 12.5$ Å, which gives $v_{oop} \approx 84$ meV Å. It is worth noting that the observed in-plane spin wave velocity in the study [9] on the similar compound with $\epsilon = 0.4$ is $v_{ip} \approx 360$ meV Å with $J \equiv J_{\text{eff}} \approx 18.8$ meV. This clearly indicates that the particular mixture of stripe and CB units following the incommensurability plays an important role to modify the in-plane spin wave velocity of the magnetic excitations.

IV. CONCLUSION

In summary, three-dimensional anisotropic magnetic excitations have been directly evidenced using INS at 10 K in half-doped $Pr_{1.5}Sr_{0.5}NiO_4$. All the experimental observations are in good agreement with the LSWT-based calculation considering the unconventional body-centered-like DCSS model of two-layer stacking of NiO_2 planes along the crystallographic c axis. The salient difference in the static DCSS unit cell representing different underlying spin microstructure with a combination of 1/3-stripe and CB units leads to different in-plane effective exchange interactions resulting in

different in-plane spin wave velocities. Consideration of out-of-plane interaction, even though it is weaker than in-plane interactions, might be decisive to have more insight into the characteristics of spin wave dispersion in 214-type nickelates. Our study indicates that the presence of three-dimensional spin dynamics at least in Pr-based 214 nickelates is seemingly ubiquitous near the half-doped region and motivates to explore the interesting aspects of magnetic excitations in the doping range near 1/3- and 1/4-stripe phases. In general our findings encourage to reinvestigate for possible three-dimensional magnetic excitations in other families of 214 nickelates.

The data sets for the inelastic neutron scattering experiment on the time-of-flight spectrometer MAPS are available from the ISIS facility, Rutherford Appleton Laboratory data portal [30]. The data sets for the inelastic neutron scattering experiment on the thermal triple-axis spectrometer PUMA are available from the corresponding authors upon reasonable request.

ACKNOWLEDGMENTS

A. Maity would like to greatly acknowledge the support of G. Eckold for giving the opportunity to use internal neutron beamtime at the instrument PUMA, FRM II, operated by Georg-August-Universität Göttingen in cooperation with Technische Universität München. R.D., A. Maity, and A. Marsicano would like to thank M. Ceretti for her kind support in the single crystal growth. R.D and A. Maity would like to acknowledge the financial support of Institut für Kristallographie, RWTH Aachen Universität, and Technische Universität München, respectively, for performing the experiments at MAPS, ISIS.

[1] J. J. Wagman, G. Van Gastel, K. A. Ross, Z. Yamani, Y. Zhao, Y. Qiu, J. R. D. Copley, A. B. Kallin, E. Mazurek, J. P. Carlo, H. A. Dabkowska, and B. D. Gaulin, Phys. Rev. B **88**, 014412 (2013).

[2] M. Hücker, H.-H. Klauss, and B. Büchner, Phys. Rev. B **70**, 220507(R) (2004).

[3] M. E. Ghazi, P. D. Spencer, S. B. Wilkins, P. D. Hatton, D. Mannix, D. Prabhakaran, A. T. Boothroyd, and S.-W. Cheong, Phys. Rev. B **70**, 144507 (2004).

[4] P. G. Freeman, A. T. Boothroyd, D. Prabhakaran, C. D. Frost, M. Enderle, and A. Hiess, Phys. Rev. B **71**, 174412 (2005).

[5] R. Kajimoto, K. Ishizaka, H. Yoshizawa, and Y. Tokura, Phys. Rev. B **67**, 014511 (2003).

[6] S.-H. Lee, Y.-C. Lai, C.-H. Du, A. F. Siegenfeld, Y.-J. Kao, P. D. Hatton, D. Prabhakaran, Y. Su, and D.-J. Huang, Phys. Rev. B **92**, 205114 (2015).

[7] M. Hepting, L. Chaix, E. W. Huang, R. Fumagalli, Y. Y. Peng, B. Moritz, K. Kummer, N. B. Brookes, W. C. Lee, M. Hashimoto, T. Sarkar, J.-F. He, C. R. Rotundu, Y. S. Lee, R. L. Greene, L. Braicovich, G. Ghiringhelli, Z. X. Shen, T. P. Devereaux, and W. S. Lee, Nature **563**, 374 (2018).

[8] M. Hücker, M. v. Zimmermann, R. Klingeler, S. Kiele, J. Geck, S. N. Bakehe, J. Z. Zhang, J. P. Hill, A. Revcolevschi, D. J. Buttrey, B. Büchner, and J. M. Tranquada, Phys. Rev. B **74**, 085112 (2006).

[9] A. Maity, R. Dutta, and W. Paulus, Phys. Rev. Lett. **124**, 147202 (2020).

[10] O. Wahyudi, M. Ceretti, I. Weill, A. Cousson, F. Weill, M. Meven, M. Guerre, A. Villesuzanne, J.-M. Bassat, and W. Paulus, CrystEngComm **17**, 6278 (2015).

[11] O. Sobolev and J. T. Park, J. Large-Scale Res. Facil. **1**, A13 (2015).

[12] R. A. Ewings, J. R. Stewart, T. G. Perring, R. I. Bewley, M. D. Le, D. Raspino, D. E. Pooley, G. Škoro, S. P. Waller, D. Zacek, C. A. Smith, and R. C. Riehl-Shaw, Rev. Sci. Instrum. **90**, 035110 (2019).

[13] See Supplemental Material at http://link.aps.org/supplemental/10.1103/PhysRevB.102.165130 for details of the neutron-scattering experiments and data analysis, macroscopic magnetic properties, comparison of magnetic intensity in the ideal and nonideal body-centered-like DCSS unit cell using the SPINW code, and effect of out-of-plane magnetic interaction on the spin dynamics, which includes Refs. [9,11,12,18,19,23,24] .

[14] R. Ewings, A. Buts, M. Le, J. van Duijn, I. Bustinduy, and T. Perring, Nucl. Instrum. Methods Phys. Res., Sect. A **834**, 132 (2016).

[15] R. Zhong, B. L. Winn, G. Gu, D. Reznik, and J. M. Tranquada, Phys. Rev. Lett. **118**, 177601 (2017).

[16] J. M. Tranquada, D. J. Buttrey, V. Sachan, and J. E. Lorenzo, Phys. Rev. Lett. **73**, 1003 (1994).

[17] S. Anissimova, D. Parshall, G. D. Gu, K. Marty, M. D. Lumsden, S. Chi, J. A. Fernandez-Baca, D. L. Abernathy, D. Lamago, J. M. Tranquada, and D. Reznik, Nat. Commun. **5**, 3467 (2014).

[18] G. Eckold and O. Sobolev, Nucl. Instrum. Methods Phys. Res., Sect. A **752**, 54 (2014).

[19] S. Toth and B. Lake, J. Phys.: Condens. Matter **27**, 166002 (2015).

[20] A. T. Boothroyd, D. Prabhakaran, P. G. Freeman, S. J. S. Lister, M. Enderle, A. Hiess, and J. Kulda, Phys. Rev. B **67**, 100407(R) (2003).

[21] A. M. Merritt, D. Reznik, V. O. Garlea, G. D. Gu, and J. M. Tranquada, Phys. Rev. B **100**, 195122 (2019).

[22] E. C. Andrade and M. Vojta, Phys. Rev. Lett. **109**, 147201 (2012).

[23] X. Batlle, X. Obradors, and B. Martinez, Phys. Rev. B **45**, 2830 (1992).

[24] X. Batlle, X. Obradors, M. J. Sayagues, M. Vallet, and J. Gonzalez-Calbet, J. Phys.: Condens. Matter **4**, 487 (1992).

[25] M. Medarde, J. Rodríguez-Carvajal, B. Martínez, X. Batlle, and X. Obradors, Phys. Rev. B **49**, 9138 (1994).

[26] K. Nakajima, K. Yamada, S. Hosoya, Y. Endoh, M. Greven, and R. J. Birgeneau, Z. Phys. B **96**, 479 (1995).

[27] J.-I. Igarashi, Phys. Rev. B **46**, 10763 (1992).

[28] S. Chakravarty, B. I. Halperin, and D. R. Nelson, Phys. Rev. B **39**, 2344 (1989).

[29] S. Chakravarty, B. I. Halperin, and D. R. Nelson, Phys. Rev. Lett. **60**, 1057 (1988).

[30] https://doi.org/10.5286/ISIS.E.RB1920233-1.